3D Trajectory Optimization for Energy-Efficient UAV Communication: A Control Design Perspective

Bin Li, *Senior Member, IEEE,* Qingliang Li, Yong Zeng, *Member, IEEE,* Yue Rong, *Senior Member, IEEE,* Rui Zhang, *Fellow, IEEE*

Abstract—This paper studies the three-dimensional (3D) trajectory optimization problem for unmanned aerial vehicle (UAV) aided wireless communication. Existing works mainly rely on the kinematic equations for UAV's mobility modeling, while its dynamic equations are usually missing. As a result, the planned UAV trajectories are piece-wise line segments in general, which may be difficult to implement in practice. By leveraging the concept of state-space model, a control-based UAV trajectory design is proposed in this paper, which takes into account both the UAV's kinematic equations and the dynamic equations. Consequently, smooth trajectories that are amenable to practical implementation can be obtained. Moreover, the UAV's controller design is achieved along with the trajectory optimization, where practical roll angle and pitch angle constraints are considered. Furthermore, a new energy consumption model is derived for quad-rotor UAVs, which is based on the voltage and current flows of the electric motors and thus captures both the consumed energy for motion and the energy conversion efficiency of the motors. Numerical results are provided to validate the derived energy consumption model and show the effectiveness of our proposed algorithms.

Index Terms—UAV communication, quad-rotor UAV, trajectory optimization, control theory.

I. INTRODUCTION

RECENTLY, unmanned aerial vehicle (UAV) aided wireless communications have received significant attentions in both academia and industry [1]–[4]. Thanks to their flexible deployment, UAVs can be used as aerial communication platforms for offering on-demand communications services from the sky, e.g., for disaster relief and temporary events. In addition, UAV-aided communication is regarded as an indispensable component not only for the future space-air-ground integrated network [5]–[8], but also for the beyond-5G (B5G) wireless networks [9]–[13].

B. Li and Q. Li are with School of Aeronautics and Astronautics, Sichuan University, Chengdu, 610065, China, e-mail: bin.li@scu.edu.cn; liqingliang@stu.scu.edu.cn.

Y. Zeng is with National Mobile Communications Research Laboratory, Southeast University, Nanjing 210096, China, and also with the Purple Mountain Laboratories, Nanjing 211111, China, e-mail: yong_zeng@seu.edu.cn.

Y. Rong is with Department of Electrical and Computer Engineering, Curtin University, GPO Box U1987, Perth, WA 6845, Australia, e-mail: y.rong@curtin.edu.au

R. Zhang is with the Department of Electrical and Computer Engineering, National University of Singapore, Singapore 117583, Singapore, e-mail: elezhang@nus.edu.sg.

A. Motivation and Prior Work

By exploiting the new design degree of freedom (DoF) offered by UAV's flexible mobility, trajectory optimization for UAV-aided communications has been extensively studied [14]–[20] for improving the communication performance. However, most of existing works in the literature assume that the UAVs fly in a two-dimensional (2D) horizontal plane [14]–[19]. In addition, they mainly rely on the kinematic equations to model the UAV mobility, while ignoring its dynamic equations. By treating UAV as a point mass, kinematic equations mainly aim to describe the motion (position, velocity and acceleration) of the UAV. In contrast, with dynamic equations, the rigid body characteristic of UAVs is taken into account, and the relationship between the forces and the motion is explicitly modeled. Since the kinematic equations do not consider the forces that generate the motion, the resulting designed trajectory is difficult to be directly implemented in practice. To resolve this issue, in this paper, both the kinematic and dynamic equations are considered, and the forces that generate the motion are chosen as the design variables. Therefore, by implementing the designed forces over time, the corresponding trajectories are practically implementable by existing UAV controllers.

On the other hand, energy efficiency is one of the most important performance measures for UAV-aided communications, which is fundamentally due to UAV's limited on-broad energy and hence finite aerial endurance [15]–[20]. A mathematical framework for designing energy-efficient UAV communication was first proposed in [15], in which an analytical energy consumption model in terms of the UAV's velocity and acceleration was derived for fixed-wing UAVs. The energy-efficient UAV communication design was then extended to rotary-wing UAVs in [16], where the energy consumption of rotary-wing UAVs was derived as a function of the flying speed. There are three components in the above energy models, namely, the induced power, the blade profile power, and the parasite power. Such energy models have been widely utilized for energy-efficient UAV communication designs in the literature. For instance, a UAV-enabled wireless powered cooperative mobile edge computing (MEC) system was considered in [17], based on the energy model derived in [15], where the UAV is capable of harvesting energy from the radio frequency (RF) signals. By adopting the energy consumption model in [16], a robust resource allocation algorithm design was investigated in [18], by jointly optimizing the UAV trajectory and the transmit beamforming vector.

In [19], multiple UAVs were assigned to collect data from a

group of sensor nodes (SNs) on the ground, and it studied the fundamental tradeoff between the aerial cost, which is defined as the propulsion energy consumption and operation costs of all UAVs, and the ground cost, which is defined as the energy consumption of all SNs. In [20], the three-dimensional (3D) trajectory optimization for the UAV was investigated. A 3D energy consumption model was proposed in [20] by assuming that the UAV moves smoothly with a small acceleration and the cruising speed is a constant. Under this assumption, [20] decomposes the power consumptions of the UAV into three components, which are vertical flight power, level flight power and drag power.

It is worth mentioning that all the aforementioned works [14]–[20] rely on the kinematic equations to model the UAV mobility, while ignoring the dynamic equations. Therefore, the resulting optimized trajectory is not directly related to the forces that drive the UAV to track the trajectory in practice. As a result, a separate controller needs to be designed to obtain the required control input for UAV motors based on the optimized UAV trajectory, as illustrated in Fig. 1(a). Moreover, under the existing design framework, UAV trajectories are usually discretized into finite piecewise line segments separated by the way-points, and the velocity and acceleration within each line segment are assumed to be constants. Under such an approach, in order to accurately characterize the actual UAV trajectories that are smooth in practice, the required number of discretized line segments needs to be sufficiently large, which becomes prohibitive as UAVs travel over long distance in practice. Fig. 2 plots the planned trajectory and the real trajectory with the existing design approach in Fig. 1(a). As shown in Fig. 2, the planned trajectory cannot be exactly followed due to the ignorance of UAV dynamics. In contrast, the proposed design does not have such an issue, as will be shown by the numerical examples in Section IV.
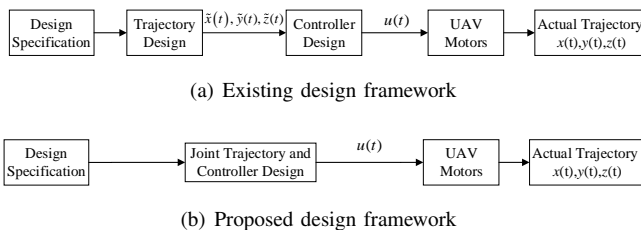

(a) Existing design framework

(b) Proposed design framework

Fig. 1. The proposed versus existing design framework for UAV trajectory in wireless communications.

B. Contributions

In this paper, we study the 3D trajectory optimization for UAV-aided communication systems based on both kinematic and dynamic equations. A new framework that seamlessly integrates trajectory planning and UAV control is proposed. With our proposed design framework, the control signals are directly obtained with the optimized trajectory, as illustrated in Fig. 1(b).

Furthermore, a new energy consumption model is derived for the commonly used quad-rotor UAVs. Different from the well-known energy model in [16], which models the required
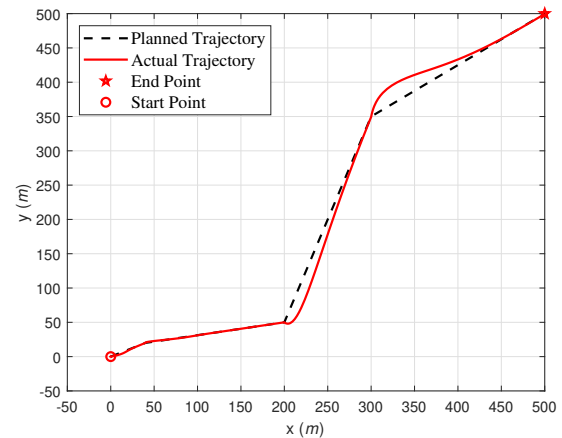

Fig. 2. The planned trajectory and actual trajectory by the existing design framework.

energy in terms of the UAV's flying velocity to support the UAV's flight status, the proposed energy model is directly derived from the voltage and current flows of the electric motors of the UAV. Therefore, it takes into account not just the UAV consumed energy as in [15], [16], but also the energy conversion efficiency of the electrical motors.

By leveraging the state-space model in control theory [21], the flying time minimization problem and the energy minimization problem are formulated as two optimal control problems, subject to various constraints with respect to the communication quality-of-service (QoS) requirement, target destination, maximum angular velocity of the motors, minimum allowable flying altitude, as well as maximum possible roll and pitch angles.

Since the design variables reside in continuous time-valued functions rather than vectors with a finite dimension, the formulated problems essentially involve infinite optimization variables. The control parametrization approach [22]–[24] is efficient for solving this type of problem. Its main idea lies in converting the infinite-dimensional optimization problem into a standard nonlinear program, which is achieved by parametrizing the control function into a finite dimensional vector and providing the gradients for the objective and constraint functions. Based on this approach, a control-based trajectory design is proposed for UAV-aided wireless communication in this paper. The pertinent gradient formulas are also derived. Since the kinematic and dynamic equations therein are solved as differential equations, the optimized trajectories are smooth curves rather than piece-wise line segments as in the aforementioned prior works. The roll- and pitch-angle constraints are also difficult to handle, since they are infinite dimensional in nature. A constraint transcription method [22] together with a local smoothing technique [22] are introduced for converting the infinite dimensional constraints into constraints of finite dimension. There are off-the-shelf software packages available for solving such problems [25], [26].

There are a wide range of potential applications for the considered problem. For example, by using the collected

data from its mounted sensors, the UAV can provide data-harvesting applications. However, data processing techniques usually require high computation power, which is difficult to afford by the UAV due to its limited payload. To overcome this issue, the UAV may offload such task to a ground server or ground terminal (GT), which has more powerful computing resources.

The main contributions of this paper are summarized as follows:

- Inspired by the modern control theory, we propose a new framework for trajectory design in UAV communication systems utilizing both kinematic and dynamic equations for UAV mobility modeling. As a result, the designed UAV trajectories are smooth curves, rather than piecewise line segments as in most existing works [16]. Furthermore, different from existing models where the UAV speed is assumed to be a constant whithin each line segment, it varies over time in general with the proposed model. In addition, the proposed model is applicable to the general 3D UAV trajectory design.
- A new energy consumption model for electrical quad-rotor UAVs is derived. Compared with that in [16], the new model is applicable to 3D trajectories. Moreover, the model is derived based on the current and voltage flow of the electrical motor. Thus, both the consumed energy on the UAV's motion and energy conversion efficiency have been taken into account.
- An integrated design framework for UAV trajectory optimization and controller design is proposed in this paper, which directly gives the control signal input to UAV motors. In contrast, a separate controller has to be designed for tracking the design trajectory in the existing works.
- An efficient algorithm is developed for the 3D trajectory optimization for mission completion time minimization and energy consumption minimization, respectively, and the required gradient formula for the objective function and the constraint functions are derived.

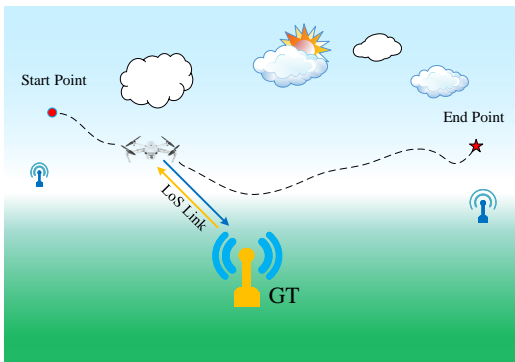## II. SYSTEM MODEL AND PROBLEM FORMULATION

Fig. 3. An illustration of UAV-aided wireless communications.

As shown in Fig. 3, we consider a UAV-aided wireless communication system. The UAV flies from a given start point

TABLE I
SYMBOL NOTATIONS

Notation	Physical Meaning
m	Aircraft mass (kg)
g	Acceleration of gravity (m/s^2)
L	Frame size (m)
I_0	No-load current (A)
U_0	No-load voltage (V)
R_0	Motor resistance (Ω)
K_v	Nominal no-load motor constant (rpm/V)
K_E	Back-electromotive force constant, $K_E \triangleq (U_0 - I_0 R_0)/(K_v U_0)$
K_T	Torque constant, $K_T \triangleq 9.55 K_E$
ω_{max}	Maximum motor speed (rad/s)
ω_i	Speed of motor i (rad/s)
N_i	Speed of motor i in revolutions per minute (rpm), $N_i \triangleq 30\omega_i/\pi$
γ_0	SNR at the reference distance of 1 meter (dB)
W	Channel bandwidth (MHz)
P_0	Communication power (W)
C_t	Thrust coefficient (N/(rad/s)^2)
C_m	Torque coefficient (N·m/(rad/s)^2)
C_d	Fuselage drag coefficient (N/(m/s)^2)
C_{dx}	Drag coefficient of x-axis (N/(m/s)^2)
C_{dy}	Drag coefficient of y-axis (N/(m/s)^2)
C_{dz}	Drag coefficient of z-axis (N/(m/s)^2)
C_{dmx}	Damping torque coefficient of x-axis (N·m/(rad/s)^2)
C_{dmy}	Damping torque coefficient of y-axis (N·m/(rad/s)^2)
C_{dmz}	Damping torque coefficient of z-axis (N·m/(rad/s)^2)
J_x	Rotational inertia of x-axis (kg·m^2)
J_y	Rotational inertia of y-axis (kg·m^2)
J_z	Rotational inertia of z-axis (kg·m^2)
J_m	Motor propeller inertia (kg·m^2)
h_{min}	Minimum safe flying altitude (m)
α	Attack angle (rad)
ϕ	Roll angle (rad)
ϕ_{max}	Safety margin for ϕ (rad)
θ	Pitch angle (rad)
θ_{max}	Safety margin for θ (rad)
ψ	Yaw angle (rad)

$\boldsymbol{q}_0$ to serve the GT, and then flies to a given end point. The UAV communicates with the GT while flying. Therefore, the flight time is equal to the data transmission time in this paper. We aim to optimize the trajectory of the UAV such that its energy consumption or flying time is minimized, while the communication QoS requirement for the GT and the dynamic constraints of the UAV are both satisfied. For convenience, the symbol notations for the main variables used in this paper are listed in Table I.
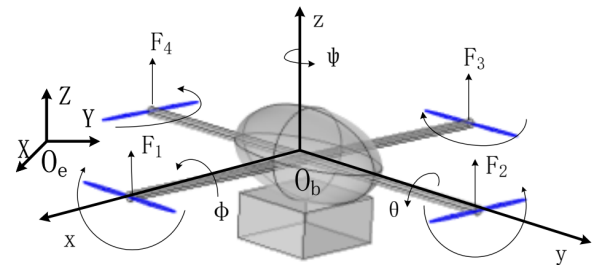
A. Dynamic Model of Quad-rotor UAV

Fig. 4. The Earth frame and fixed-body frame.

As illustrated in Fig. 4, the UAV is treated as a rigid body in this paper. In order to derive the dynamic model of the UAV,

the Earth frame and the fixed-body frame need to be defined. As shown in Fig. 4, O_e and O_b denote the Earth frame and the fixed-body frame, respectively. Let $\boldsymbol{q}(t) = [x(t)\ y(t)\ z(t)]^\top$ be the coordinates of the UAV at the Earth frame at time instant t, and $\boldsymbol{\Phi}(t) = [\phi(t)\ \theta(t)\ \psi(t)]^\top$ be the Euler angles of the UAV at the fixed-body frame at time instant t, where $[\cdot]^\top$ stands for the matrix transpose.

The thrusts at time instant t, which are denoted as $F_i(t)$, $i \in \{1,2,3,4\}$, are generated by the four electric motors as shown in Fig. 4. Two motors rotate counterclockwise, while the others rotate clockwise as illustrated in Fig. 4. Here, $\omega_i(t)$, $i \in \{1,2,3,4\}$ denote the angular velocities of the motors shaft at t. According to [27], for each motor $i \in \{1,2,3,4\}$,

$$F_i(t) = C_t \omega_i^2(t), \tag{1}$$

where C_t is the constant thrust coefficient.

According to [28], [29], the dynamic model of the quad-rotor UAV is given in (2) shown on the top of the next page. In (2), $\Omega(t) = \omega_1(t) - \omega_2(t) + \omega_3(t) - \omega_4(t)$ and $\mathrm{sign}(a)$ denotes the sign of a.

B. Energy Consumption Model

We consider a UAV equipped with four battery-powered brushless motors. For each motor $i = 1,2,3,4$, the current $I_i(t)$ and the voltage $U_i(t)$ at each time instant t are given by [30]

$$I_i(t) = \frac{C_m}{K_T} \omega_i^2(t) + I_0, \tag{3}$$

$$U_i(t) = K_E N_i(t) + I_i(t) R_0. \tag{4}$$

Thus, for each motor $i = 1,2,3,4$, the power consumption of the motor can be obtained

$$\begin{aligned} P_i(t) &= U_i(t) I_i(t) \\ &= c_4 \omega_i^4(t) + c_3 \omega_i^3(t) + c_2 \omega_i^2(t) + c_1 \omega_i(t) + c_0, \end{aligned} \tag{5}$$

where

$$c_0 = I_0^2 R_0, \ c_1 = 30 K_E I_0 / \pi, \ c_2 = 2 C_m R_0 I_0 / K_T,$$
$$c_3 = 30 C_m K_E / (\pi K_T), \ c_4 = C_m^2 R_0 / K_T^2.$$

The total energy consumption of the UAV over time $t \in [0, T]$ can be expressed by

$$E(t) = \int_0^t \left(\sum_{i=1}^4 P_i(\tau) + P_0 \right) \mathrm{d}\tau, \tag{6}$$

where T is the total aerial endurance (or flying time for convenience) of the UAV, which is assumed to be a variable in this paper. In practical cases, P_0 is usually much less than $\sum_{i=1}^4 P_i(\tau)$.

C. Channel Model

The probabilistic LoS channel model from [31] is adopted here. We denote $\boldsymbol{p} = [p_x\ p_y\ p_z]^T \in \mathbb{R}^{3 \times 1}$ as the position of the GT. According to [31], the channel coefficient between the UAV and GT $h(t)$ can be expressed by

$$h(t) = \sqrt{\beta(t)} \tilde{h}(t), \tag{7}$$

where $\beta(t)$ accounts for the large-scale fading effects (e.g. path loss and shadowing) and $\tilde{h}(t)$, which is a complex-valued random variable with $\mathbb{E}\left[\left|\tilde{h}(t)\right|^2\right] = 1$, accounts for the small-scale fading.

Considering the occurrence probability of LoS and non-LoS (NLoS), $\beta(t)$ can be expressed as

$$\beta(t) = \begin{cases} \beta_0 d^{-\tilde{\alpha}}(t), & \text{LoS link} \\ \kappa \beta_0 d^{-\tilde{\alpha}}(t), & \text{NLoS link,} \end{cases} \tag{8}$$

where $\beta_0 = \left(\frac{\lambda}{4\pi}\right)^2$ denotes the channel power at the reference distance of 1 meter (m), λ is the carrier wavelength, $\tilde{\alpha}$ is the path loss exponent, $\kappa < 1$ is the additional attenuation factor due to the NLoS condition, and $d(t) = \|\boldsymbol{q}(t) - \boldsymbol{p}\|$ is the distance between the UAV and GT at time instant $t \in [0, T]$. The probability of LoS occurrence can be modeled as the following sigmoid function [31]

$$P_{\text{LoS}}(t) = \frac{1}{1 + a \exp\left(-b\left[\tilde{\theta}(t) - a\right]\right)}, \tag{9}$$

where a and b are parameters that depend on the propagation environment and $\tilde{\theta}(t) = \frac{180}{\pi} \arcsin\left(\frac{z(t) - p_z}{d(t)}\right)$ is the elevation angle.

Obviously, the probability of NLoS is $P_{\text{NLoS}}(t) = 1 - P_{\text{LoS}}(t)$. Then, the expected channel power gain is

$$\begin{aligned} \mathbb{E}\left[|h(t)|^2\right] &= P_{\text{Los}}(t) \beta_0 d^{-\tilde{\alpha}}(t) + (1 - P_{\text{LoS}}(t)) \kappa \beta_0 d^{-\tilde{\alpha}}(t) \\ &= \hat{P}_{\text{LoS}}(t) \beta_0 d^{-\tilde{\alpha}}(t), \end{aligned} \tag{10}$$

where $\hat{P}_{\text{LoS}}(t) = \kappa + (1 - \kappa) P_{\text{LoS}}(t)$ represents the regularized LoS probability.

The achievable communication rate between UAV and GT can be expressed as

$$R(t) = W \log_2 \left(1 + \frac{P_0 |h(t)|^2}{\sigma^2 \Gamma_0} \right), \tag{11}$$

where W is the bandwidth, P_0 is the transmit power, σ^2 is the noise power at the receiver, and $\Gamma_0 > 1$ accounts for the channel capacity loss due to the practical modulation and coding scheme. Then, according to [16], [32], the accumulated communication throughput $Q(t)$ between the UAV and the GT at t can be written as

$$\begin{aligned} Q(t) &= \int_0^t \mathbb{E}\left[R(t)\right] \mathrm{d}\tau \\ &\leq \int_0^t W \log_2 \left(1 + \frac{P_0 \mathbb{E}\left[|h(\tau)|^2\right]}{\sigma^2 \Gamma_0} \right) \mathrm{d}\tau \\ &= \int_0^t W \log_2 \left(1 + \frac{\gamma_0 \hat{P}_{\text{LoS}}(\tau)}{\|\boldsymbol{q}(\tau) - \boldsymbol{p}\|^{\tilde{\alpha}}} \right) \mathrm{d}\tau, \tag{12} \end{aligned}$$

where $\gamma_0 = P_0 \beta_0 / (\sigma^2 \Gamma_0)$.

$$
\begin{bmatrix}
m\ddot{x}(t) \\
m\ddot{y}(t) \\
m\ddot{z}(t) \\
J_x\ddot{\phi}(t) \\
J_y\ddot{\theta}(t) \\
J_z\ddot{\psi}(t)
\end{bmatrix}
=
\begin{bmatrix}
C_t \sum_{i=1}^{4} \omega_i^2(t) \left[\sin\phi(t)\sin\psi(t) + \sin\theta(t)\cos\phi(t)\cos\psi(t) \right] - \text{sign}(\dot{x}(t))C_{dx}\dot{x}^2(t) \\
C_t \sum_{i=1}^{4} \omega_i^2(t) \left[\sin\theta(t)\sin\psi(t)\cos\phi(t) - \sin\phi(t)\cos\psi(t) \right] - \text{sign}(\dot{y}(t))C_{dy}\dot{y}^2(t) \\
C_t \sum_{i=1}^{4} \omega_i^2(t)\cos\phi(t)\cos\theta(t) - mg - \text{sign}(\dot{z}(t))C_{dz}\dot{z}^2(t) \\
LC_t \left[\omega_2^2(t) - \omega_4^2(t) \right] + (J_y - J_z)\dot{\theta}(t)\dot{\psi}(t) - J_m\Omega(t)\dot{\theta}(t) - \text{sign}(\dot{\phi}(t))C_{dmx}\dot{\phi}^2(t) \\
LC_t \left[\omega_3^2(t) - \omega_1^2(t) \right] + (J_z - J_x)\dot{\phi}(t)\dot{\psi}(t) + J_m\Omega(t)\dot{\phi}(t) - \text{sign}(\dot{\theta}(t))C_{dmy}\dot{\theta}^2(t) \\
C_m \left[\omega_1^2(t) - \omega_2^2(t) + \omega_3^2(t) - \omega_4^2(t) \right] + (J_x - J_y)\dot{\phi}(t)\dot{\theta}(t) - \text{sign}(\dot{\psi}(t))C_{dmz}\dot{\psi}^2(t)
\end{bmatrix}
\tag{2}
$$

D. The UAV State-Space Model

According to the modern control theory [21], a dynamic system is modeled as a set of differential equations, and it can be expressed in the form of the state-space model. A state-space model consists of state variables and control variables, and the operations of the system are governed by the states. The state variables cannot be changed directly. Instead, they are usually steered to the desired value by manipulating the control variables accordingly.

By observing the dynamic model in (2) and considering the physical meaning of the variables therein, we define the state vector as

$$
\boldsymbol{x}(t) = \Big[x(t)\ y(t)\ z(t)\ \dot{x}(t)\ \dot{y}(t)\ \dot{z}(t)\ \phi(t)\ \theta(t)\ \psi(t)
$$
$$
\dot{\phi}(t)\ \dot{\theta}(t)\ \dot{\psi}(t)\ E(t)\ Q(t) \Big]^\top
$$

and the control vector as $\boldsymbol{u}(t) = [u_1(t)\ u_2(t)\ u_3(t)\ u_4(t)]^\top$, where

$$
\begin{aligned}
u_1(t) &= \sum_{i=1}^{4} \omega_i^2(t) \\
u_2(t) &= \omega_2^2(t) - \omega_4^2(t) \\
u_3(t) &= \omega_3^2(t) - \omega_1^2(t) \\
u_4(t) &= \omega_1^2(t) - \omega_2^2(t) + \omega_3^2(t) - \omega_4^2(t).
\end{aligned}
\tag{13}
$$

The chosen control variables possess physical meanings as follows. $C_t u_1(t) = \sum_{i=1}^{4} F_i(t)$ is the total thrust force on the UAV. $LC_t u_2(t)$, $LC_t u_3(t)$ and $C_m u_4(t)$ are the generated torques on the x axis, y axis and z axis, respectively. In fact, $\omega_i^2(t)$, $i = 1, 2, 3, 4$ can be obtained by $u_i(t)$, $i = 1, 2, 3, 4$ with the following equations:

$$
\begin{aligned}
\omega_1(t) &= 0.5 \left(u_1(t) + u_4(t) - 2u_3(t) \right)^{0.5} \\
\omega_2(t) &= 0.5 \left(u_1(t) - u_4(t) + 2u_2(t) \right)^{0.5} \\
\omega_3(t) &= 0.5 \left(u_1(t) + u_4(t) + 2u_3(t) \right)^{0.5} \\
\omega_4(t) &= 0.5 \left(u_1(t) - u_4(t) - 2u_2(t) \right)^{0.5}.
\end{aligned}
\tag{14}
$$

Then, the state-space model of system (2) can be written as (15) shown on the top of the next page. In (15), the power of the ith motor $P_i(t)$ can be obtained by substituting $\omega_i(t)$ in (14) into (5). For notational simplicity, (15) is more compactly written as

$$
\dot{\boldsymbol{x}}(t) = \boldsymbol{f}_1\left(\boldsymbol{x}(t), \boldsymbol{u}(t)\right),
\tag{16}
$$

where $\dot{\boldsymbol{x}}(t)$ denotes the derivative of $\boldsymbol{x}$ with respect to t.

REMARK 1 The functions of motor angular velocities in (13) are chosen as the control variables, which can be directly implemented in practical systems. This is because by setting

the angular velocities of the motors at each time instant $t \in [0, T]$, the UAV can fly towards the destination along any desired trajectory.

E. Problem Formulation

Next, the trajectory optimization problems are formulated as optimal control problems by considering two different performance measures - flying time and energy consumption.

1) Flying time minimization: The time-optimal control problem for the UAV-aided wireless communications can be formulated as follows.

$$
\textbf{P1}: \quad \min_{\boldsymbol{u}(t), T}\ T
$$
$$
\begin{aligned}
s.t.\quad &C_0:\ \dot{\boldsymbol{x}}(t) = \boldsymbol{f}_1\left(\boldsymbol{x}(t), \boldsymbol{u}(t)\right),\ t \in [0, T] \\
&C_1:\ 0 \le u_1(t) \le U_{1max},\ t \in [0, T] \\
&C_2:\ |u_i(t)| \le U_{imax},\ i = 2, 3, 4,\ t \in [0, T] \\
&C_3:\ \boldsymbol{x}(0) = \boldsymbol{x}_0 \\
&C_4:\ x_1(T) = x_F \\
&C_5:\ x_2(T) = y_F \\
&C_6:\ x_3(T) = z_F \\
&C_7:\ x_{14}(T) \ge Q_{min} \\
&C_8:\ x_3(t) \ge h_{min},\ t \in [0, T] \\
&C_9:\ |x_7(t)| \le \phi_{max},\ t \in [0, T] \\
&C_{10}:\ |x_8(t)| \le \theta_{max},\ t \in [0, T].
\end{aligned}
$$

The main difference of the above optimal control problem from conventional trajectory optimization problems (e.g. [14]–[20]) is that the dynamic equations in C_0 are considered. Hence, it is also called dynamic optimization. Another difference is that the decision variables of an optimal control problem are continuous instead of being discretized as in [14]–[16].

C_1 is introduced to limit the angular velocities of the motors, while C_2 is imposed to limit their differences. C_3 gives the initial value for the state vector $\boldsymbol{x}(t)$, which is necessary for computing the differential equations in (16). Constraints $C_4 - C_6$ specify the destination location requirement. Note that by dropping the constraints, $C_4 - C_6$, the formulated problem corresponds to the scenario that the destination point is also part of the optimization variables, for which the techniques proposed below can be directly applied. For safety reasons, constraints $C_8 - C_{10}$ are imposed to limit the flying altitude, the roll angle and the pitch angle of the UAV, where h_{min} is the minimum allowable altitude, ϕ_{max} and θ_{max} are the safety margin for $\phi(t)$ and $\theta(t)$, respectively. Q_{min} is the minimum communication throughput requirement for GT.

$$\begin{cases} \dot{x}_1(t) = x_4(t), \ \dot{x}_2(t) = x_5(t), \ \dot{x}_3(t) = x_6(t), \\ \dot{x}_4(t) = \left[C_t u_1(t) \left(\sin x_7(t) \sin x_9(t) + \sin x_8(t) \cos x_7(t) \cos x_9(t) \right) - \mathrm{sign}(x_4(t)) C_{dx} x_4^2(t) \right] / m, \\ \dot{x}_5(t) = \left[C_t u_1(t) \left(\sin x_8(t) \sin x_9(t) \cos x_7(t) - \sin x_7(t) \cos x_9(t) \right) - \mathrm{sign}(x_5(t)) C_{dy} x_5^2(t) \right] / m, \\ \dot{x}_6(t) = \left[C_t u_1(t) \left(\cos x_7(t) \cos x_8(t) \right) - mg - \mathrm{sign}(x_6(t)) C_{dz} x_6^2(t) \right] / m, \\ \dot{x}_7(t) = x_{10}(t), \ \dot{x}_8(t) = x_{11}(t), \ \dot{x}_9(t) = x_{12}(t), \\ \dot{x}_{10}(t) = \left[L C_t u_2(t) + (J_y - J_z) x_{11}(t) x_{12}(t) - J_m \Omega(t) x_{11}(t) - \mathrm{sign}(x_{10}(t)) C_{dmx} x_{10}^2(t) \right] / J_x, \\ \dot{x}_{11}(t) = \left[L C_t u_3(t) + (J_z - J_x) x_{10}(t) x_{12}(t) + J_m \Omega(t) x_{10}(t) - \mathrm{sign}(x_{11}(t)) C_{dmy} x_{11}^2(t) \right] / J_y, \\ \dot{x}_{12}(t) = \left[C_m u_4(t) + (J_x - J_y) x_{10}(t) x_{11}(t) - \mathrm{sign}(x_{12}(t)) C_{dmz} x_{12}^2(t) \right] / J_z, \\ \dot{x}_{13}(t) = \sum_{i=1}^{4} P_i(t) + P_0, \\ \dot{x}_{14}(t) = W \log_2 \left(1 + \frac{\gamma_0 \hat{P}_{\mathrm{LoS}}(t)}{\left[(x_1(t) - p_x)^2 + (x_2(t) - p_y)^2 + (x_3(t) - p_z)^2 \right]^{\bar{\alpha}/2}} \right). \end{cases} \quad (15)$$

2) Energy consumption minimization:
Similarly, the energy minimization problem can be cast as follows.

$$\mathbf{P2}: \quad \min_{\boldsymbol{u}(t), T} \quad x_{13}(T)$$
$$s.t. \quad C_0 - C_{10}.$$

The only difference between P1 and P2 is the objective function. In P2, the objective function is $x_{13}(T)$, which is the energy cost up to the mission completion time T ($E(T)$) according to the definition of $\boldsymbol{x}(t)$. P2 aims to find $\boldsymbol{u}(t)$ and T such that the energy cost of the UAV is minimized while the end point constraint, the kinematic and dynamic equations of the UAV, the flying altitude constraint, the roll angle constraint, the pitch angle constraint, and the minimum communication throughput requirement are satisfied.

REMARK 2 Compared with the destination constraints $C_4 - C_6$, the state constraints $C_8 - C_{10}$, which are also known as path constraints, are more difficult to handle, since they involve an infinite number of constraints to satisfy over the time horizon $[0, T]$ [22].

F. Special Cases

In the last subsection, we first consider two special cases of the above formulated problems, for fly-hover-fly trajectory and 2D trajectory optimization, respectively.

1) Fly-hover-fly trajectory: Fly-hover-fly trajectory is commonly used for UAV communications [16], which is easier to implement in practice. Under this scheme, the UAV first flies directly to a location above the GT, where it hovers and communicates with the GT. After this, it flies directly to the end point. In particular, the UAV flies horizontally with a fixed flying velocity from the start to the hovering location and from it to the end location. As a result, the flying time and the energy consumption mainly depend on the flying velocity.

We first consider the case when the UAV is in the level flight mode with a constant speed V_c, for which the four brushless motors rotate in the same constant speed ω_c. For illustration, the forces on the aircraft in this scenario are shown in Fig. 5, where F is the thrust force generated by the four motors, D is the drag force, α is the angle of attack, and $\bar{F}$ is the projection of F on the horizontal plane.

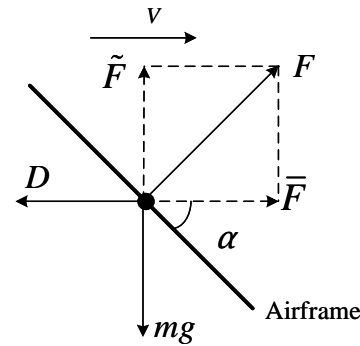
Fig. 5. The forces on the UAV during the level flight with a constant speed V_c.

According to (1) and [27], [29], we have

$$F = 4 C_t \omega_c^2, \ D = C_d V_c^2, \quad (17)$$

where C_d is the fuselage drag coefficient. Since the UAV's speed is constant, we have

$$\tilde{F} = F \cos(\alpha) = mg, \ \bar{F} = F \sin(\alpha) = D. \quad (18)$$

The angular speed of the motor ω_c can be solved from equations (17) and (18), given by

$$\omega_c = \sqrt{\frac{mg}{4 C_T}} \left(1 + \frac{C_d^2}{m^2 g^2} V_c^4 \right)^{\frac{1}{4}}. \quad (19)$$

It then follows from (5) that the flying power consumption of the UAV can be obtained as

$$P_c = 4 \left(c_4 \omega_c^4 + c_3 \omega_c^3 + c_2 \omega_c^2 + c_1 \omega_c + c_0 \right). \quad (20)$$

By substituting (19) into (20), the power consumption P_c can be expressed in terms of the cruising speed V_c, given by

$$P_c = \frac{c_4}{4} \left(\frac{m^2 g^2}{C_t^2} + \frac{C_d^2}{C_t^2} V_c^4 \right) + \frac{c_3}{2} \left(\frac{m^2 g^2}{C_t^2} + \frac{C_d^2}{C_t^2} V_c^4 \right)^{\frac{3}{4}}$$
$$+ c_2 \left(\frac{m^2 g^2}{C_t^2} + \frac{C_d^2}{C_t^2} V_c^4 \right)^{\frac{1}{2}} + 2 c_1 \left(\frac{m^2 g^2}{C_t^2} + \frac{C_d^2}{C_t^2} V_c^4 \right)^{\frac{1}{4}}$$
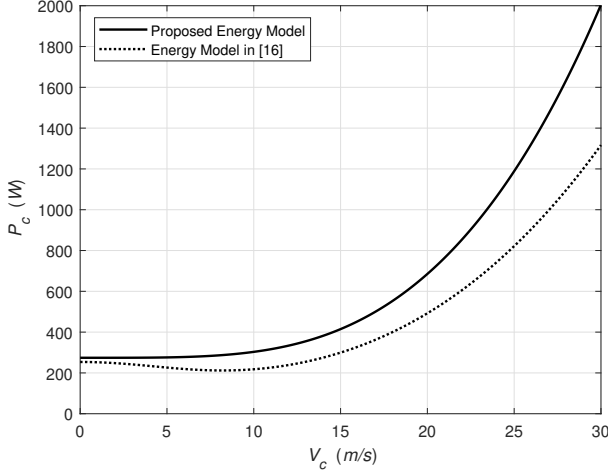$$+ 4 c_0, \quad (21)$$

Fig. 6. The power consumption P_c versus cruising speed V_c.

which is plotted in Fig. 6.

It is observed from (21) that at high flying speed $V_c \gg 1$, the power increases with V_c in a quartic manner. This is different from the cubic relationship derived in [16]. Such a difference is mainly due to the fact that the model in (21) is directly derived based on the current and voltage flows of the electrical motors, and thus it takes into account not just the required power to support the UAV flight status, as in [16], but also the energy conversion efficiency of the electrical motors. According to [30], the output power of the electric motor can be modeled as

$$\tilde{P}_c = 4M\omega_c = 4C_m \left(\frac{mg}{4C_T} \right)^{3/2} \left(1 + \frac{C_d^2}{m^2 g^2} V_c^4 \right)^{\frac{3}{4}}, \quad (22)$$

where $M = C_m \omega_c^2$ is the propeller torque. It is observed from (22) that similar to [16], the output power is a function of V_c with cubic order. Moreover, the energy model in [16] is also drawn in Fig. 6, and the parameters in the model are obtained from the UAV model in this paper. It is worth mentioning that while the energy consumption model in [16] is applicable for generic rotary-wing UAVs, the models in (21) and (22) are derived for electric quad-rotor UAVs specifically.

Ignoring the energy consumption and time of UAV in the acceleration and deceleration of flat flight, the total flying time of fly-hover-fly trajectory is

$$T_{tot} = T_1 + T_h + T_2 = \frac{D_1}{V_c} + \frac{Q_{min}}{W \log_2 \left(1 + \frac{\gamma_0 \bar{P}_{LoS}}{D_h^{\bar{\alpha}}} \right)} + \frac{D_2}{V_c}, \quad (23)$$

where T_1 denotes the flying time from the start point to the hovering location, T_h is the hovering time, T_2 denotes the flying time from the hovering location to the end point, D_1 represents the distance between the start point and GT, D_2 is the distance between the GT and the end point, D_h denotes the distance between GT and the hovering location, $\bar{P}_{LoS}$ is

the regularized LoS probability at the hovering point. Then, the total energy consumption can be expressed by

$$E_{tot} = P_c T_1 + (P_h + P_0)T_h + P_c T_2, \quad (24)$$

where P_h is the hovering power, which is obtained by setting $V_c = 0$ in (19) and (20), and P_0 is the communication power.
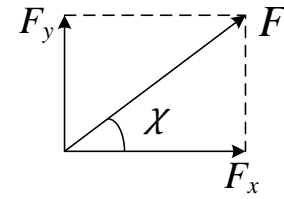

Fig. 7. The two components of $\bar{F}$ for the level flight.

2) 2D trajectory optimization: In this case, the UAV flies horizontally with a time-varying velocity $\boldsymbol{V}(t) = [v_x(t) \ v_y(t)]^\top$, where $v_x(t)$ and $v_y(t)$ are the flying velocities on the x axis and y axis of the Earth frame, respectively.

In this scenario, $\tilde{F} = mg$ and $\bar{F} = mg \tan(\alpha)$ by observing the forces on the UAV in Fig. 5. Then, we project $\bar{F}$ onto the x axis and y axis of the Earth frame as shown in Fig. 7, where χ is called the heading angle. From (18), it follows that $\bar{F} = mg \tan(\alpha)$.

Then, by applying Newton's second law and considering the definition of the drag force D in (17), it follows that

$$\begin{aligned} ma_x &= F_x - D_x = mg \tan(\alpha) \cos(\chi) - C_d |v_x| v_x, \\ ma_y &= F_y - D_y = mg \tan(\alpha) \sin(\chi) - C_d |v_y| v_y, \end{aligned} \quad (25)$$

where a_x, a_y, D_x and D_y are the accelerations and drag force on the x axis and y axis, respectively.

Defining the state vector as $\boldsymbol{x}(t) = [x(t) \ y(t) \ v_x(t) \ v_y(t) \ Q(t) \ E(t)]^\top$ and the control vector as $\boldsymbol{u}(t) = [\alpha(t) \ \chi(t)]^\top$, respectively, then the 2D version of the state-space model (15) can be written as

$$\begin{cases} \dot{x}_1(t) = x_3(t), \ \dot{x}_2(t) = x_4(t), \\ \dot{x}_3(t) = g \tan(u_1(t)) \cos(u_2(t)) - \text{sign}(x_3(t)) \frac{C_d}{m} x_3^2(t), \\ \dot{x}_4(t) = g \tan(u_1(t)) \sin(u_2(t)) - \text{sign}(x_4(t)) \frac{C_d}{m} x_4^2(t), \\ \dot{x}_5(t) = \sum\limits_{i=1}^{4} P_i(t) + P_0, \\ \dot{x}_6(t) = W \log_2 \left(1 + \frac{\gamma_0 \hat{P}_{\text{LoS}(t)}}{((x_1(t)-q_{kx})^2+(x_2(t)-q_{ky})^2+H^2)^{\bar{\alpha}/2}} \right), \end{cases} \quad (26)$$

where $P_i(t)$ is obtained by substituting $\omega_i(t)$ in (14) into (5). Similarly, (26) is simply denoted as

$$\dot{\boldsymbol{x}}(t) = \boldsymbol{f}_2 \left(\boldsymbol{x}(t), \boldsymbol{u}(t) \right). \quad (27)$$

Thus, the 2D version of P1 can be written as

$$\begin{aligned} \textbf{P3}: \quad &\min_{\boldsymbol{u}(t),T} \quad T \\ &s.t. \quad S_0: \dot{\boldsymbol{x}}(t) = \boldsymbol{f}_2 \left(\boldsymbol{x}(t), \boldsymbol{u}(t) \right), \ t \in [0,T] \\ &\qquad S_1: |u_1(t)| \le \alpha_{max}, \ t \in [0,T] \\ &\qquad S_2: \boldsymbol{x}(0) = \boldsymbol{x}_0 \\ &\qquad S_3: x_1(T) = x_T \\ &\qquad S_4: x_2(T) = y_T \\ &\qquad S_5: x_6(T) \ge Q_{min}. \end{aligned}$$

And the 2D version of P2 can be expressed

$$\textbf{P4}: \quad \min_{\boldsymbol{u}(t),T} \quad x_5(T)$$
$$s.t. \quad S_0 - S_5.$$

III. Proposed Solution

P1-P4 are optimal control problems subject to state constraints, which are challenging to solve in the control theory. Since the flying time T is also an optimization variable, then a time scaling method is introduced in this section to transform the varying time horizon into a fixed one. The decision vector $\boldsymbol{u}(t)$ is a multi-dimensional continuous-time function, which implies that there are an infinite number of decision variables. For this, a control parametrization technique is utilized to discretize the control vector $\boldsymbol{u}(t)$. Since the state constraint is infinite dimensional in nature, then a constraint transcription method together with a local smoothing technique is introduced to convert the these constraints into the constraints in an integral form. In this section, we will focus on solving P1, since P2, P3 and P4 can be solved in a similar manner.

A. Time Scaling

The following linear transform [23], [24] is applied to the dynamic systems (16) and (27) for mapping the original time horizon $[0,T]$ into a fixed time horizon $[0,1]$

$$\frac{dt}{ds} = \tan\theta = T. \tag{28}$$

Then, by applying the chain rule to (16) and (27) and considering (28), it follows that

$$\dot{\boldsymbol{x}}(s) = \frac{d\boldsymbol{x}}{ds} = \frac{d\boldsymbol{x}}{dt} \cdot \frac{dt}{ds} = T \cdot \boldsymbol{f}_i(\boldsymbol{x}(s), \boldsymbol{u}(s)), \ i = 1, 2. \tag{29}$$

The end location constraints C_4-C_7 then become

$$C_4 : x_1(1) = x_T, \ C_5 : x_2(1) = y_T, \tag{30}$$
$$C_6 : x_3(1) = z_T, \ C_7 : x_{14}(1) \geq Q_{min}. \tag{31}$$

Similarly, the state constraints C_8-C_{10} become

$$C_8 : \ x_3(s) \geq h_{min}, \ C_9 : \ |x_7(s)| \leq \phi_{max}, \tag{32}$$
$$C_{10} : \ |x_8(s)| \leq \theta_{max}, \ s \in [0,1]. \tag{33}$$
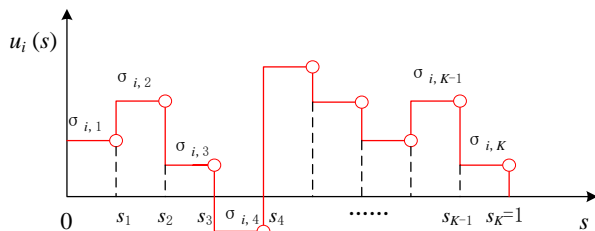
B. Control Parametrization

$u_i(s)$

Fig. 8. Control parametrization.

The time horizon $[0,1]$ is partitioned into K equal subintervals with the following $K+1$ boundary points,

$$\left\{ s_0 = 0, s_1 = \frac{1}{K}, s_2 = \frac{2}{K}, ..., s_{K-1} = \frac{K-1}{K}, s_K = 1 \right\}.$$

As illustrated in Fig. 8, for each $i = 1, 2, 3, 4$, $u_i(s)$ is approximated by the following piecewise constant function [22]:

$$u_i(s) \approx \sum_{k=1}^{K} \sigma_{i,k} \Gamma_{[s_{k-1}, s_k)}(s), \tag{34}$$

where

$$\Gamma_{[s_{k-1}, s_k)}(s) = \begin{cases} 1, & s \in [s_{k-1}, s_k) \\ 0, & \text{otherwise.} \end{cases}$$

By letting $\boldsymbol{\sigma}_i = [\sigma_{i,1}, \sigma_{i,2}, \ldots, \sigma_{i,K}]^\top$, $i = 1, 2, 3, 4$ and $\boldsymbol{\sigma} = [\boldsymbol{\sigma}_1^\top, \boldsymbol{\sigma}_2^\top, \boldsymbol{\sigma}_3^\top, \boldsymbol{\sigma}_4^\top]^\top$, $\boldsymbol{u}(s)$ is thus parametrized by the vector $\boldsymbol{\sigma}$.

By replacing $\boldsymbol{u}(s)$ with $\boldsymbol{\sigma}$, the dynamic equations in (29) are simply denoted as

$$\dot{\boldsymbol{x}}(s) = T \cdot \boldsymbol{f}_i(\boldsymbol{x}(s), \boldsymbol{\sigma}), \ i = 1, 2. \tag{35}$$

Considering the control parametrization (34), constraint C_1 is rewritten as

$$C_1 : \ 0 \leq \sigma_{1,k} \leq U_{1max}, \ k = 1, 2, \ldots, K, \tag{36}$$

and C_2 can be modified in a similar manner.

REMARK 3 Control parametrization does not mean 'control discretization', though the piece-wise constant functions are adopted here to approximate the control inputs as shown in Fig. 8. In fact, continuous and even differentiable control inputs can be obtained by using the piece-wise linear function and spline function to approximate the control inputs [22]. In addition, the state variables are still smooth by

C. Constraint Approximation

Considering the constraint transcription technique and local smoothing technique in [22], C_8 can be approximated by

$$\gamma + \int_0^1 l_{C_8,\epsilon} ds \geq 0, \tag{37}$$

where

$$l_{C_8,\epsilon} = \begin{cases} 0, & x_3(s) - h_{min} > \epsilon \\ -(x_3(s) - h_{min} - \epsilon)^2 / 4\epsilon, & -\epsilon \leq x_3(s) - h_{min} \leq \epsilon \\ x_3(s) - h_{min}, & x_3(s) - h_{min} < -\epsilon. \end{cases}$$

and $\gamma > 0$. C_9 and C_{10} can be handled in a similar manner, which are written below.

$$\gamma + \int_0^1 l_{C_{9-1},\epsilon} ds \geq 0, \ \gamma + \int_0^1 l_{C_{9-2},\epsilon} ds \geq 0, \tag{38}$$

$$\gamma + \int_0^1 l_{C_{10-1},\epsilon} ds \geq 0, \ \gamma + \int_0^1 l_{C_{10-2},\epsilon} ds \geq 0, \tag{39}$$

where $l_{C_{9-1},\epsilon}$, $l_{C_{9-2},\epsilon}$, $l_{C_{10-1},\epsilon}$ and $l_{C_{10-2},\epsilon}$ are obtained similarly as $l_{C_8,\epsilon}$.

D. Algorithm

By applying the transforms from the previous subsections to P1, we obtain the following problem:

$$(\mathbf{P1})_{\epsilon,\gamma}: \quad \min_{\boldsymbol{\sigma},T} \quad T$$

$$s.t. \quad C_0 : \dot{\boldsymbol{x}}(s) = T\boldsymbol{f}_1\left(\boldsymbol{x}(s),\boldsymbol{\sigma}\right), s \in [0,1]$$

$$C_1 : \ 0 \leq \sigma_{1,k} \leq U_{1max}, \ k = 1,2,\ldots,K$$

$$C_2 : \ |\sigma_{i,k}| \leq U_{imax}, \ i = 2,3,4, k = 1,2,\ldots,K$$

$$C_3 : \ \boldsymbol{x}(0) = \boldsymbol{x}_0$$

$$C_4 : \ x_1(1) = x_T$$

$$C_5 : \ x_2(1) = y_T$$

$$C_6 : \ x_3(1) = z_T$$

$$C_7 : \ x_{14}(1) \geq Q_{min}$$

$$C_8 : \ \gamma + \int_0^1 l_{C_8,\epsilon}\mathrm{d}s \geq 0$$

$$C_9 : \ \gamma + \int_0^1 l_{C_{9-1},\epsilon}\mathrm{d}s \geq 0, \ \gamma + \int_0^1 l_{C_{9-2},\epsilon}\mathrm{d}s \geq 0$$

$$C_{10} : \ \gamma + \int_0^1 l_{C_{10-1},\epsilon}\mathrm{d}s \geq 0, \ \gamma + \int_0^1 l_{C_{10-2},\epsilon}\mathrm{d}s \geq 0.$$

Problem $(\mathrm{P1})_{\epsilon,\gamma}$ can be solved as a nonlinear program, if the gradients of the objective function and constraints functions are available. This can be verified by the following arguments.

At iteration k, the current decision vector is denoted as $\boldsymbol{\sigma}^{(k)}$. Then, we construct $\boldsymbol{u}^{(k)}(s)$ with $\boldsymbol{\sigma}^{(k)}$ according to (34) and solve the differential equations $\dot{\boldsymbol{x}}^{(k)}(s) = T^{(k)}\boldsymbol{f}_1\left(\boldsymbol{x}^{(k)}(s),\boldsymbol{u}^{(k)}(s)\right), \ s \in [0,1]$ for $\boldsymbol{x}^{(k)}(s)$. Hence, the values of the constraint functions $C_3 - C_{10}$ can be obtained with $\boldsymbol{x}^{(k)}(s)$ and $\boldsymbol{u}^{(k)}(s)$. Since the value of the objective function is known, which is $T^{(k)}$, the problem can be regarded as a nonlinear program as long as the gradients of the objective function and the constraint functions are available. To this end, the gradient formula will be derived in the next subsection. The main procedures for solving problem $(\mathrm{P1})_{\epsilon,\gamma}$ are summarized in Algorithm 1.

Algorithm 1 For Solving Problem $(\mathrm{P1})_{\epsilon,\gamma}$ at iteration k

---

Input: $\boldsymbol{\sigma}^{(k)}$ and $T^{(k)}$.
Output: $\boldsymbol{\sigma}^{(k+1)}$ and $T^{(k+1)}$.
1: Construct $\boldsymbol{u}^{(k)}(s)$ with $\boldsymbol{\sigma}^{(k)}$ according to (34).
2: Solve $\dot{\boldsymbol{x}}^{(k)}(s) = T^{(k)}\boldsymbol{f}_1\left(\boldsymbol{x}^{(k)}(s),\boldsymbol{u}^{(k)}(s)\right), \ s \in [0,1]$ for $\boldsymbol{x}^{(k)}(s)$ with $\boldsymbol{u}^{(k)}(s)$.
3: Calculate the values of the constraint functions C_3-C_{10} with $\boldsymbol{x}^{(k)}(s)$ and $\boldsymbol{u}^{(k)}(s)$.
4: Calculate the gradients of the objective function and the constraint functions with $\boldsymbol{x}^{(k)}(s)$ and $\boldsymbol{u}^{(k)}(s)$.
5: Input the values and the gradients of objective functions and the constraint functions to the nonlinear program solver.
6: Output $\boldsymbol{\sigma}^{(k+1)}$ and $T^{(k+1)}$.

In order to solve problem P1, we shall solve a sequence of problems $(\mathrm{P1})_{\epsilon,\gamma}$ by adjusting ϵ and γ as shown in Algorithm 2. As summarized in Algorithm 2, ε and γ determine the accuracy and the feasibility of the algorithm, respectively. The

initial γ is set as $\varepsilon/16$ for guaranteeing the convergence of the algorithm [22]. γ is usually initialized to be slightly larger in order to find a feasible solution. As $\varepsilon \to 0$, which is achieved by setting $\varepsilon = \varepsilon/10$ in Step 4, $\boldsymbol{\sigma}_{\varepsilon,\gamma}$ and $T_{\varepsilon,\gamma}$ converge to the optimal solution $\boldsymbol{\sigma}^*$ and T^*, respectively. In fact, $\gamma \to 0$ as $\varepsilon \to 0$ and this is achieved by setting $\gamma = \gamma/10$ in Step 4.

Algorithm 2 For Solving Problem P1

Input: $\boldsymbol{\sigma}_0$ and T_0.
Output: $\boldsymbol{\sigma}^*$ and T^*.
Initialization: ε, $\gamma = \frac{\varepsilon}{16}$, ε_{min}, $\boldsymbol{\sigma} = \boldsymbol{\sigma}_0$, and $T = T_0$.
1: **while** $\varepsilon \geq \varepsilon_{min}$ **do**
2:     Solve problem $(\mathrm{P1})_{\epsilon,\gamma}$ with $\boldsymbol{\sigma}$ and T as initial point and output $\boldsymbol{\sigma}_{\varepsilon,\gamma}$ and $T_{\varepsilon,\gamma}$.
3:     **if** C_8, C_9 and C_{10} are satisfied **do**
4:         Set $\varepsilon = \varepsilon/10$, $\gamma = \gamma/10$, $\boldsymbol{\sigma} = \boldsymbol{\sigma}_{\varepsilon,\gamma}$, $T = T_{\varepsilon,\gamma}$.
5:     **else**
6:         Set $\gamma = \gamma/2$.
7:     **end if**
8: **end while**
9: Output $\boldsymbol{\sigma}^* = \boldsymbol{\sigma}$ and $T^* = T$.

REMARK 4 Let $\boldsymbol{u}^*(s)$ and $\boldsymbol{u}^*_{\varepsilon,\gamma}(s)$ (constructed by $\boldsymbol{\sigma}^*_{\varepsilon,\gamma}$ and $T^*_{\varepsilon,\gamma}$ according to (34)) be an optimal solution to problem P1 and that to problem $(\mathrm{P1})_{\epsilon,\gamma}$, respectively. Then, as $\varepsilon \to 0$ and the number of time intervals $K \to \infty$, $\boldsymbol{u}^*_{\varepsilon,\gamma}(s) \to \boldsymbol{u}^*(s)$. For more details of the proof, the readers may refer to Theorems 9.2.1, 9.2.2 and 9.2.3 of [22].

REMARK 5 The subproblem of solving problem $(\mathrm{P1})_{\epsilon,\gamma}$ with the sequential quadratic programming (SQP) method is a quadratic program, and its computational complexity is $O\left(K^2\right)$. Therefore, the computational cost increases with the number of time slots, K. Thus, there is a trade-off between the performance and complexity in choosing K. In practice, K is usually set as 10. This is because the performance improvement is marginal if $K > 10$.

REMARK 6 The solutions of P2-P4 can be obtained in a similar manner as that for P1. For P2, the only difference is the objective function. Therefore, Algorithm 2 can be applied to P2 by changing the objective function and the corresponding gradients. P3 and P4 are simplified versions of P1 and P2, respectively, with less state equations in S_0 and less constraints. Thus, Algorithm 2 can be applied to them by solving state equations with lower dimensions and fewer number of constraints.

REMARK 7 The developed framework can be extended to the multi-UAV or multi-user scenario, for which the problem will be a mixed integer non-convex optimal control problem. The integer decision variables, which are due to communication scheduling, might be tackled by the benders decomposition method or the relaxation technique in [33]. The non-convexity caused by the co-channel interferences can be handled by techniques like successive convex approximation [33]. More in-depth study on multi-UAV and multi-user setups will be left as future work.

TABLE II
THE PARAMETERS OF THE UAV AND EXPERIMENT RELATED PARAMETERS

m	3	ω_{max}	640	C_t	4.848×10^{-5}
g	9.8	K_v	380	C_m	8.891×10^{-7}
L	0.3	γ_0	60	C_{dmx}	0.016
I_0	0.3	W	1	C_{dmy}	0.016
U_0	10	P_0	5	C_{dmz}	0.1
R_0	0.4	C_{dx}	0.11	J_x	4.29×10^{-2}
h_{min}	60	C_{dy}	0.11	J_y	4.29×10^{-2}
ϕ_{max}	1	C_{dz}	0.2	J_z	7.703×10^{-2}
θ_{max}	1	-	-	J_m	8.02×10^{-4}

E. Gradient Formula

Last, since the gradients are essential for implementing Algorithm 1, the gradient formula for the objective function are derived in this subsection. The gradient formula for the constraint functions can be derived in a similar manner and thus are omitted for brevity.

Theorem 1 The gradient formula of the objective function J are

$$\frac{\partial J}{\partial \boldsymbol{\sigma}} = T \int_0^1 \left[\frac{\partial \boldsymbol{f}_1(\boldsymbol{x}(s), \boldsymbol{\sigma})}{\partial \boldsymbol{\sigma}} \right]^\top \boldsymbol{\lambda}_0(s) \mathrm{d}s, \qquad (40)$$

$$\frac{\partial J}{\partial T} = 1 + \int_0^1 \boldsymbol{\lambda}_0^\top(s) \boldsymbol{f}_1(\boldsymbol{x}(s), \boldsymbol{\sigma}) \mathrm{d}s, \qquad (41)$$

where $\boldsymbol{\lambda}_0(s)$ is the solution of the following co-state equation

$$\dot{\boldsymbol{\lambda}}_0(s) = -T \left[\frac{\partial \boldsymbol{f}_1(\boldsymbol{x}(s), \boldsymbol{\sigma})}{\partial \boldsymbol{x}} \right]^\top \boldsymbol{\lambda}_0(s) \qquad (42)$$

with the terminating condition $\boldsymbol{\lambda}_0(1) = \boldsymbol{0}$.

Proof: See Appendix A.

IV. NUMERICAL RESULTS

In this section, the proposed power consumption model of the motor is firstly verified by experimental data, and then the effectiveness of the proposed algorithm is demonstrated by simulations. The parameters of the UAV [34] and system setups are given in Table II. The modeling parameters for the probabilistic LoS channel model in (8) and (9) are set as $a = 10$, $b = 0.6$, $\kappa = 0.2$, and $\tilde{\alpha} = 2.3$ [16]. The coordinates of the end point is $\boldsymbol{q}_F = [x_F, y_F, z_F]^T = [500, 500, 100]^T$ and that of the GT is $\boldsymbol{p} = [p_x, p_y, p_z]^T = [200, 400, 0]^T$. The cruising speed for the fly-hover-fly trajectory is set as $V_c = 13 \ m/s$.

A. Verification of Proposed Motor Power Consumption Model

The experimental data are obtained from the vendor's website [35], which are given in Table III. We plot the motor power consumption versus the motor rotation speed with the experimental data and the proposed model (5) in Fig. 9. As shown in Fig. 9, the proposed model fits well with the experimental data, which verifies the effectiveness of the motor's power consumption model in (5).
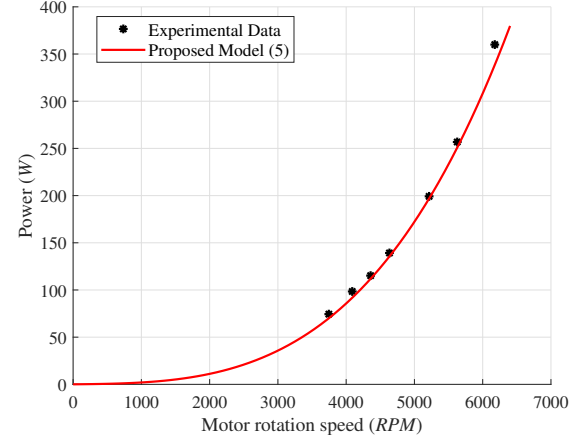
Fig. 9. Comparison of experimental data and proposed model.

B. Example 1: 2D Trajectory Optimization

In this example, the UAV flies in the horizontal plane with fixed altitude of $100 \ m$. The initial condition for P3 and P4 is set as $\boldsymbol{x}_0 = [0, 0, 10, 10, 0, 0]^\top$. We set $K = 20$ for implementing Algorithm 1.

We plot the time and energy minimizing trajectories with $Q_{min} = 100 \ Mbits$ and $500 \ Mbits$ in Fig. 10. The trajectory under the fly-hover-fly scheme is also plotted in Fig. 10 for comparison. As illustrated in Fig. 10, the trajectories get closer to the GT as Q_{min} increases. This is expected since it takes more time and energy for the UAV to finish the communication task for a larger Q_{min}.

In addition, we observe that the time and energy minimizing trajectories (denoted by Min Time and Min Energy, respectively) almost coincide under each QoS constraint as shown in Fig. 10. This is due to the limitation of the 2D trajectory design, and we shall show later that it is not the case for the 3D trajectory design.

The flying time and energy consumption for each scenario are given in Fig. 14. As expected, the time optimized trajectories outperform the other trajectories in terms of minimum flying time, and energy optimized trajectories outperform the other trajectories in terms of minimum energy consumption.

C. Example 2: 2D Trajectory Optimization under Different Energy Models

In this example, we compare the performance of the proposed energy model with the state-of-the-art model in [16]. Since the energy model in [16] is only applicable to 2D UAV trajectory, the problem setting in Example 1 is adopted here for simplicity. We plot the optimized 2D trajectories, the flying speed versus time, and the energy consumption versus the throughput requirement with the two models in Fig. 11. Here, 'Real Cost [16]' stands for the energy cost of the optimized trajectory obtained according to [16], which is calculated by the proposed energy model. It is observed from Fig. 11(a) and Fig. 11(b) that with the energy model in [16], the UAV flies around the GT. By contrast, with the proposed model, it hovers on the top of the GT. This is because the optimal

TABLE III
DATA OF THE BRUSHLESS MOTOR WITH PROPELLER (MODEL:1550) [35]

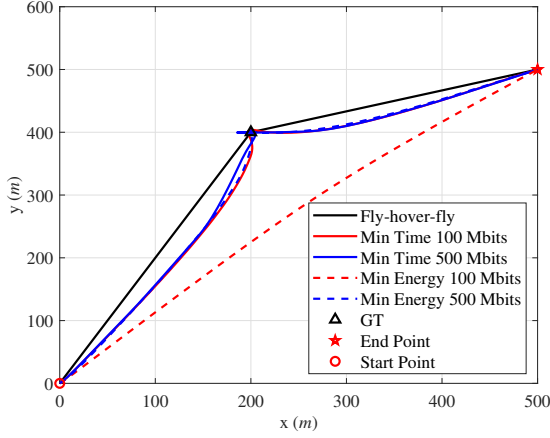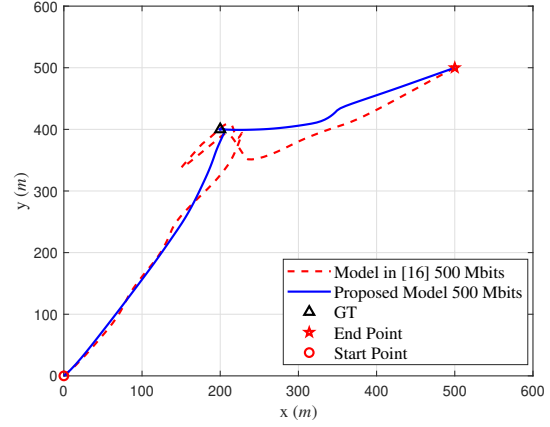| Speed (rpm)	3746	4089	4358	4634	5215	5627	6177
Power (W)	74.4	98.4	115.2	139.2	199.2	256.8	360.0

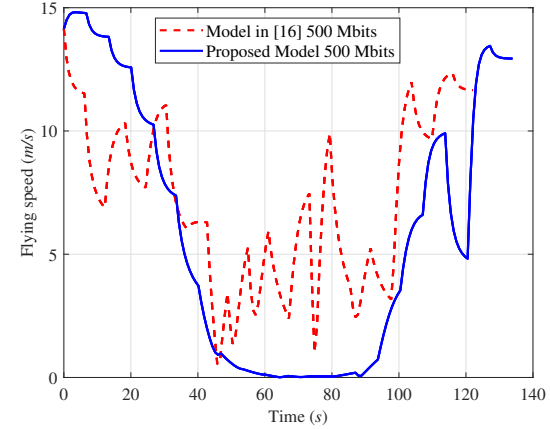Fig. 10. Example 1: the optimized 2D trajectories.

speed for minimum power consumption of the proposed model corresponds to the hovering status, while that for the model in [16] corresponds to a non-zero speed, as shown in Fig. 6. In addition, it is also observed from Fig. 11(b) that the change in speed with the proposed model is smoother than that with the model in [16]. As expected, the energy consumption of the proposed model is lower than the true value and it is higher than the theoretical value of that in [16], as illustrated in Fig. 11(c).

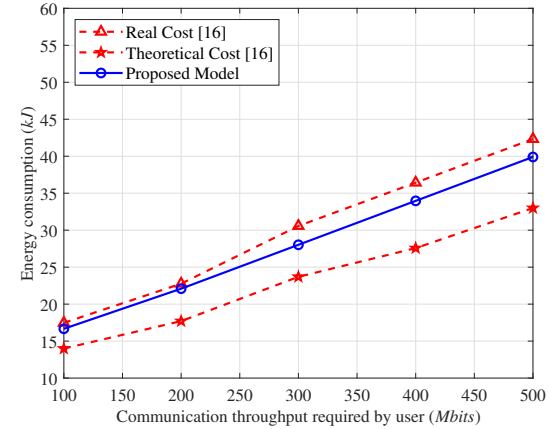### D. Example 3: 3D Trajectory Optimization

In this example, the 3D trajectory optimization is considered. The initial condition for P1 and P2 is set as $x_0 = [0, 0, 100, 10, 10, 0, -0.98, 0.04, -0.76, 0, 0, 0, 0, 0]^\top$ and K is set as 20.

The time and energy minimizing trajectories with $Q_{min} = 100$ $Mbits$ or 500 $Mbits$ are plotted in Fig. 12. For comparison, the trajectory generated under the fly-hover-fly scheme is also plotted. As expected, the altitudes of trajectories with more QoS requirements are lower and closer to the GT as shown in Fig. 12. Different from the 2D trajectory design, the time minimizing trajectory is quite different from the energy minimizing trajectory under the same QoS constraint.

The flying altitude and flying speed versus time are also plotted in Fig. 13. Fig. 13(a) further verifies that the altitudes of trajectories with more QoS requirements are lower. Interestingly, we can observe that the UAV even files at the lowest allowable altitude for more than 20 s on the top of GT for the 'Energy Min 500 $Mbits$' case. This is expected since the communication channel is the best with the minimum altitude. In Fig. 13(b), we observe that the time optimized trajectories increase the flying speed dramatically initially. This is because the UAV has to get closer to the GT more quickly in order to reduce the flying time.

(a) The optimized 2D trajectories.

(b) The flying speed versus time.

(c) Mission completion time versus throughput.

Fig. 11. Example 2: 2D trajectory optimization with different energy models.
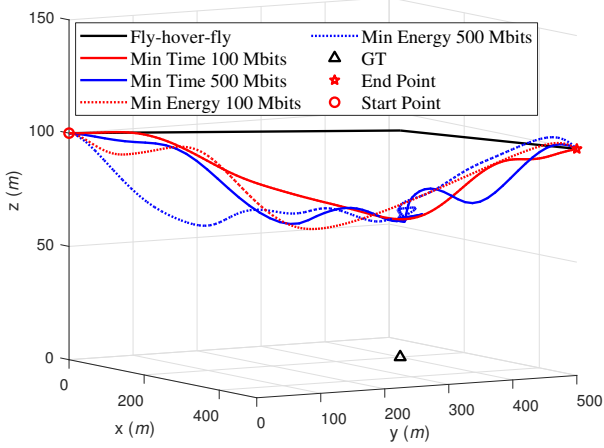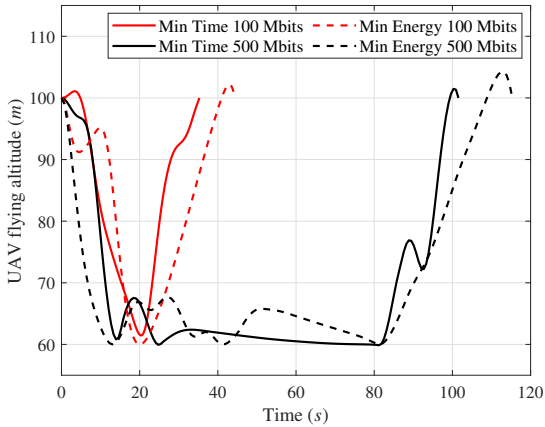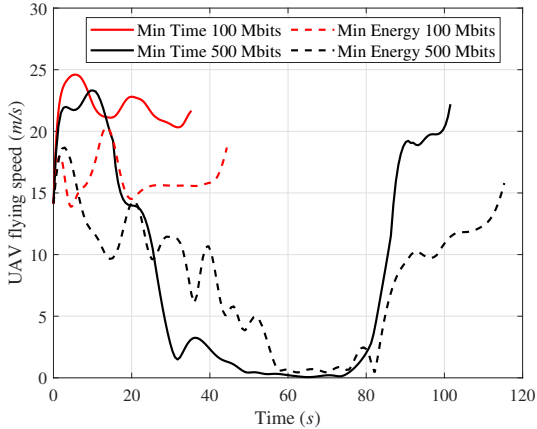
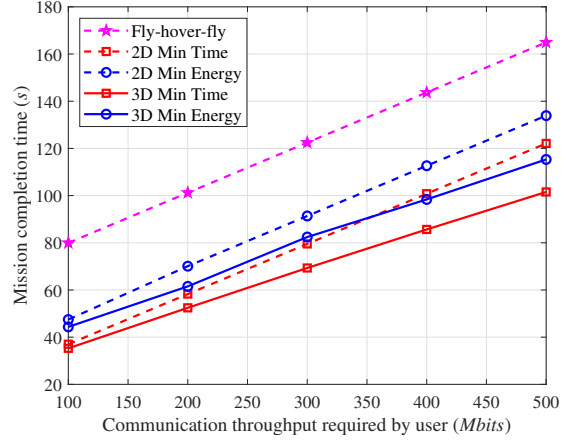Fig. 12. Example 3: the optimized 3D trajectories.


(a) Mission completion time versus throughput requirement.

(b) Energy consumption versus throughput requirement.

Fig. 14. Example 3: Performance versus throughput requirement.

(a) Flying altitude versus time.

(b) Flying speed versus time.

Fig. 13. Example 3: flying altitude and speed.

In order to illustrate the performance gain of the 3D trajectory optimization over 2D trajectory optimization, we plot the completion time and the energy cost versus the communication throughput in Fig. 14(a) and Fig. 14(b), respectively. As shown in Fig. 14(a), the 3D time optimized trajectories take less time than those of the 2D trajectories with the same communication throughput. Similarly, the 3D energy minimization trajectories cost less energy than those of the 2D trajectories with the same communication throughput.

E. Example 4: 3D Trajectory Optimization without End Point Constraints

In this example, we consider a scenario of Example 3, in which the destination of the UAV is not fixed, but part of the optimization variables, by dropping constraints C_4, C_5 and C_6 in P1 and P2. The optimized 3D trajectories and the corresponding flying speeds are plotted in Fig. 15(a) and Fig. 15(b), respectively. It is observed that without fixing the end point, the UAV completes the task when it is still hovering above the GT. This is because with the proposed model, the hovering status ($V_c = 0$) costs the least energy according to Fig. 6 and also enjoys the strongest channel.
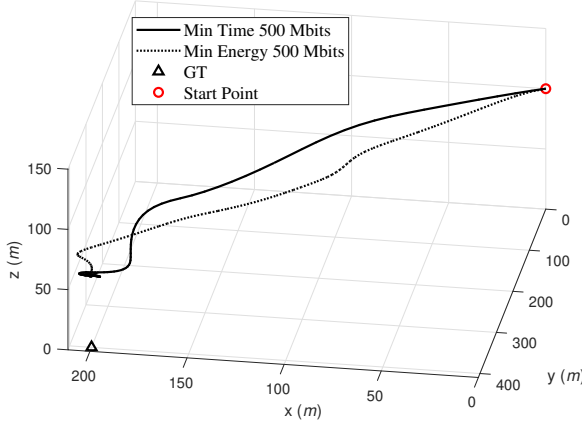
(a) The optimized 3D trajectories.
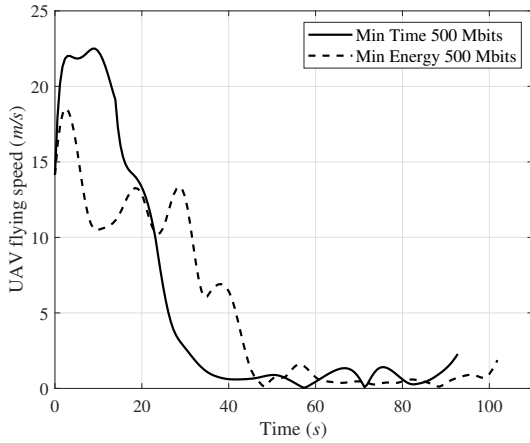
(b) Flying speed versus time.

Fig. 15.   Example 4: 3D trajectory optimization without end point constraints.

F. Example 5: Trade-off Between Performance and Complexity

In oder to examine the trade-off between the performance and the complexity (in terms of number of time partition intervals) of the proposed algorithm, we provide the objective values of P3 and P4 with different K in Table IV. In this example, the altitude of the UAV is 100 m. The initial condition is set as $\boldsymbol{x}_0 = [0, 0, 10, 10, 0, 0]^\top$ and $Q_{min} = 500$ $Mbits$. As illustrated in Table IV, the improvement of the objective value is only notable for K increasing from 3 to 6 and it becomes negligible for $K \geq 6$. Therefore, $K = 20$ is large enough for ensuring the performance and K is usually set as 10 in practice [24].

V. Conclusion

A new control-based UAV trajectory optimization approach was proposed in this paper based on the concept of state-space models. Compared to prior works in this line of research, the dynamic equations of UAVs were considered and as a result, the optimized trajectory constitutes smooth curves that can be easily implemented in practice. Moreover, an integrated design was proposed, which simultaneously optimizes the trajectory and output control signals for the UAV. In addition, a new energy consumption model for electric quad-rotor UAVs was proposed, based on which a practical 3D trajectory optimization algorithm was developed. Different from the existing UAV energy models, the proposed model was derived directly based on the voltage and current flows of the UAV's electric motors, which takes into account the energy conversion efficiency. Numerical results demonstrated the effectiveness of our proposed algorithms for both 2D and 3D UAV trajectory optimization.

Appendix A
Proof of Theorem 1

We consider a standard optimal parameter selection problem P. The dynamic system is given as

$$
\begin{aligned}
\dot{x}(t) &= \boldsymbol{f}\left(t, \boldsymbol{x}(t), \boldsymbol{\xi}\right), \\
\boldsymbol{x}(0) &= \boldsymbol{x}_0(\boldsymbol{\xi}).
\end{aligned}
\tag{43}
$$

The goal of problem P is to find a $\boldsymbol{\xi} \in \mathbb{R}^s$ such that the cost function

$$
g_0(\boldsymbol{\xi}) = \Phi_0\left(\boldsymbol{x}(T|\boldsymbol{\xi}), \boldsymbol{\xi}\right) + \int_0^T L_0\left(t, \boldsymbol{x}(t|\boldsymbol{\xi}), \boldsymbol{\xi}\right)\mathrm{d}t \tag{44}
$$

is minimized subject to the equality constraints

$$
g_i(\boldsymbol{\xi}) = \Phi_i\left(\boldsymbol{x}(T|\boldsymbol{\xi}), \boldsymbol{\xi}\right) + \int_0^T L_i\left(t, \boldsymbol{x}(t|\boldsymbol{\xi}), \boldsymbol{\xi}\right)\mathrm{d}t = 0, \tag{45}
$$

$i = 1, 2, ..., N_e$, and inequality constraints

$$
g_i(\boldsymbol{\xi}) = \Phi_i\left(\boldsymbol{x}(T|\boldsymbol{\xi}), \boldsymbol{\xi}\right) + \int_0^T L_i\left(t, \boldsymbol{x}(t|\boldsymbol{\xi}), \boldsymbol{\xi}\right)\mathrm{d}t \geq 0, \tag{46}
$$

$i = N_e + 1, N_e + 2, ..., N_e + N$. Then, the gradient formulas for the cost function and the constraint functions of problem P are given in the following lemma.

Lemma 1: (Theorem 7.2.2 in [22]) Considering problem P, for each $i = 0, 1, 2, ..., N_e + N$, the gradient of the cost/constraint function is given by

$$
\begin{aligned}
\frac{\partial g_i(\boldsymbol{\xi})}{\partial \boldsymbol{\xi}} = {} & \frac{\partial \Phi_i\left(\boldsymbol{x}(T|\boldsymbol{\xi}), \boldsymbol{\xi}\right)}{\partial \boldsymbol{\xi}} + \boldsymbol{\lambda}_0^T(0|\boldsymbol{\xi}) \frac{\partial \boldsymbol{x}_0(\boldsymbol{\xi})}{\partial \boldsymbol{\xi}} + \\
& \int_0^T \frac{\partial H_i\left(t, \boldsymbol{x}(t|\boldsymbol{\xi}), \boldsymbol{\xi}, \boldsymbol{\lambda}_i(t|\boldsymbol{\xi})\right)}{\partial \boldsymbol{\xi}}\mathrm{d}t,
\end{aligned}
$$

where

$$
H_i\left(t, \boldsymbol{x}(t|\boldsymbol{\xi}), \boldsymbol{\xi}, \boldsymbol{\lambda}_i(t|\boldsymbol{\xi})\right) = L_i\left(t, \boldsymbol{x}(t), \boldsymbol{\xi}\right) + \boldsymbol{\lambda}_i(t)^\top \boldsymbol{f}(\boldsymbol{x}(t), \boldsymbol{\xi})
$$

is the corresponding Hamiltonian and $\boldsymbol{\lambda}_i(t)$ is the corresponding co-state vector satisfying the following differential equations:

$$
\left(\dot{\boldsymbol{\lambda}}_i(t)\right)^\top = -\frac{\partial H_i\left(t, \boldsymbol{x}(t|\boldsymbol{\xi}), \boldsymbol{\xi}, \boldsymbol{\lambda}_i(t|\boldsymbol{\xi})\right)}{\partial \boldsymbol{x}}
$$

with

$$
\left(\boldsymbol{\lambda}_i(T)\right)^\top = \frac{\partial \Phi_i\left(\boldsymbol{x}(T|\boldsymbol{\xi})\right)}{\partial \boldsymbol{x}}.
$$

To prove Theorem 1, we define the corresponding Hamiltonian as

$$
H_0\left(\boldsymbol{x}(s), \boldsymbol{\lambda}_0(s), \boldsymbol{u}(s), T\right) = T\boldsymbol{\lambda}_0^\top \boldsymbol{f}_1(\boldsymbol{x}(s), \boldsymbol{u}(s)). \tag{47}
$$

TABLE IV
EXAMPLE 3: THE TRADE-OFF BETWEEN THE PERFORMANCE AND K

	K	3	6	10	15	20
Time Min	Time (s)	202.737	125.033	123.573	122.265	122.105
Energy Min	Energy (kJ)	42.261	40.214	40.004	39.929	39.899

Then, we take the derivative of (47) with respect to $\boldsymbol{u}$ and T, which yields

$$\frac{\partial H_0}{\partial \boldsymbol{u}} = T \left[\frac{\partial \boldsymbol{f}_1\left(\boldsymbol{x}(s), \boldsymbol{u}(s)\right)}{\partial \boldsymbol{u}} \right]^\top \boldsymbol{\lambda}_0(s),$$
$$\frac{\partial H_0}{\partial T} = \boldsymbol{\lambda}_0(s)^\top \boldsymbol{f}_1\left(\boldsymbol{x}(s), \boldsymbol{u}(s)\right). \tag{48}$$

Since $\Phi_0\left(\boldsymbol{x}(T)\right) = T$,

$$\frac{\partial \Phi_0}{\partial \boldsymbol{u}} = 0, \; \frac{\partial \Phi_0}{\partial T} = 1 \tag{49}$$

and $\boldsymbol{x}_0$ does not depend on $\boldsymbol{u}$ and T, we have

$$\frac{\partial \boldsymbol{x}_0}{\partial \boldsymbol{u}} = 0, \; \frac{\partial \boldsymbol{x}_0}{\partial T} = 0. \tag{50}$$

By applying Lemma 1, it follows that

$$\frac{\partial J}{\partial \boldsymbol{u}} = \frac{\partial \Phi_0}{\partial \boldsymbol{u}} + \boldsymbol{\lambda}_0^\top(0)\frac{\partial \boldsymbol{x}_0}{\partial \boldsymbol{u}} + \int_0^1 \frac{\partial H_0}{\partial \boldsymbol{u}} \mathrm{d}s. \tag{51}$$

Substituting (48), (49) and (50) into (51), we obtain

$$\frac{\partial J}{\partial \boldsymbol{u}} = T \int_0^1 \left[\frac{\partial \boldsymbol{f}_1\left(\boldsymbol{x}(s), \boldsymbol{u}\right)}{\partial \boldsymbol{u}} \right]^\top \boldsymbol{\lambda}_0(s)\mathrm{d}s, \tag{52}$$

and (41) can be derived in a similar manner, which thus completes the proof.

REFERENCES

[1] Y. Zeng, Q. Wu, and R. Zhang, "Accessing from the sky: A tutorial on UAV communications for 5G and beyond," *Proceedings of the IEEE*, vol. 107, no. 12, pp. 2327-2375, Dec. 2019

[2] A. Sharma, P. Vanjani, N. Paliwal, C. M. W. Basnayaka, D. N. K. Jayakody, H. Wang, and P. Muthuchidambaranathan, "Communication and networking technologies for UAVs: a survey," *Journal of Network and Computer Applications*, vol. 168, 2020.

[3] L. Gupta, R. Jain, and G. Vaszkun, "Survey of important issues in UAV communication networks," *IEEE Communications Surveys & Tutorials*, vol. 18, no. 2, pp. 1123-1152, 2016.

[4] M. Mozaffari, W. Saad, M. Bennis, Y. -H. Nam, and M. Debbah,"A tutorial on UAVs for wireless networks: applications, challenges, and open problems," *IEEE Communications Surveys & Tutorials*, vol. 21, no. 3, pp. 2334-2360, 2019.

[5] D. Liu, Y. Xu, J. Wang, J Chen, K Yao, Q. Wu, and A. Anpalagan, "Opportunistic UAV utilization in wireless networks: Motivations, applications, and challenges," *IEEE Communications Magazine*, vol. 58, no. 5, pp. 62-68, May 2020.

[6] A. Fotouhi, H. Qiang, M. Ding, M. Hassan, L. G. Giordano, A. Garcia-Rodriguez, and J. Yuan, "Survey on UAV cellular communications: Practical aspects, standardization advancements, regulation, and security challenges," *IEEE Communications Surveys & Tutorials*, vol. 21, no. 4, pp. 3417-3442, 2019.

[7] S. Hayat, E. Yanmaz, and R. Muzaffar, "Survey on Unmanned Aerial Vehicle networks for civil applications: A communications viewpoint," *IEEE Communications Surveys & Tutorials*, vol. 18, no. 4, pp. 2624-2661, 2016.

[8] W. Khawaja, I. Guvenc, D. W. Matolak, U. Fiebig, and N. Schneckenburger, "A survey of Air-to-Ground propagation channel modeling for Unmanned Aerial Vehicles," *IEEE Communications Surveys & Tutorials*, vol. 21, no. 3, pp. 2361-2391, 2019.

[9] A. Garcia-Rodriguez, G. Geraci, D. Lopez-Perez, L. G. Giordano, M. Ding, and E. Bjornson, "The essential guide to realizing 5G-connected UAVs with massive MIMO," *IEEE Communications Magazine*, vol. 57, no. 12, pp. 84-90, December 2019.

[10] J. Urama, R. Wiren, O. Galinina, J.i Kauppi, K. Hiltunen, J. Erkkila, F. Chernogorov, P. Etelaaho, M. Heikkila, J. Torsner, S. Andreev, and M. Valkama, "UAV-aided interference assessment for private 5G NR deployments: Challenges and solutions," *IEEE Communications Magazine*, vol. 58, no. 8, pp. 89-95, Aug. 2020.

[11] B. Li, Z. Fei, and Y. Zhang, "UAV communications for 5G and beyond: Recent advances and future trends," *IEEE Internet of Things Journal*, vol. 6, no. 2, pp. 2241-2263, Apr. 2019.

[12] S. Sekander, H. Tabassum, and E. Hossain, "Multi-tier drone architecture for 5G/B5G cellular networks: Challenges, trends, and prospects," *IEEE Communications Magazine*, vol. 56, no. 3, pp. 96-103, Mar. 2018,.

[13] M. Mozaffari, A. Taleb Zadeh Kasgari, W. Saad, M. Bennis, and M. Debbah, "Beyond 5G with UAVs: Foundations of a 3D wireless cellular network," *IEEE Transactions on Wireless Communications*, vol. 18, no. 1, pp. 357-372, Jan. 2019.

[14] Y. Zeng, R. Zhang, and T. J. Lim, "Throughput maximization for UAV-enabled mobile relaying systems," *IEEE Transactions on Communications*, vol. 64, no. 12, pp. 4983-4996, Dec., 2016.

[15] Y. Zeng and R. Zhang, "Energy-efficient UAV communication with trajectory optimization," *IEEE Transactions on Wireless Communications*, vol. 16, no. 6, pp. 3747-3760, Jun. 2017.

[16] Y. Zeng, J. Xu, and R. Zhang, "Energy minimization for wireless communication with rotary-wing UAV," *IEEE Transactions on Wireless Communications*, vol. 18, no. 4, pp. 2329-2345, Apr. 2019.

[17] Y. Liu, K. Xiong, Q. Ni, P. Fan, and K. B. Letaief, "UAV-assisted wireless powered cooperative mobile edge computing: Joint offloading, CPU control, and trajectory optimization," *IEEE Internet of Things Journal*, vol. 7, no. 4, pp. 2777-2790, Apr. 2020.

[18] D. Xu, Y. Sun, D. W. K. Ng, and R. Schober, "Multiuser MISO UAV communications in uncertain environments with no-fly zones: Robust trajectory and resource allocation design," *IEEE Transactions on Communications*, vol. 68, no. 5, pp. 3153-3172, May 2020.

[19] C. Zhan and Y. Zeng, "Aerial-ground cost tradeoff for multi-UAV-enabled data collection in wireless sensor networks," *IEEE Transactions on Communications*, vol. 68, no. 3 pp. 1937-1950, Mar. 2020.

[20] Y. Sun, D. Xu, D. W. K. Ng, L. Dai, and R. Schober, "Optimal 3D-trajectory design and resource allocation for solar-powered UAV communication systems," *IEEE Transactions on Communications*, vol. 67, no. 6, pp. 4281-4298, Jun. 2019.

[21] K. Ogata, "Modern control engineering, 5th edition" *Prentice Hall*, 2010.

[22] K. L. Teo, B. Li, C. Yu, and V. Rehbock, "Applied and computational optimal control: a control parametrization approach," *Springer*, 2021.

[23] B. Li, C.J. Yu, K.L. Teo, and G.R. Duan. "An exact penalty function method for continuous inequality constrained optimal control problem," *Journal of Optimization Theory and Applications*, vol. 151 no.2, pp. 260-291, 2011.

[24] B. Li, C. Xu, K.L. Teo, and J. Chu, "Time optimal Zermelos navigation problem with moving and fixed obstacles," *Applied Mathematics and Computation*, vol. 224, pp. 866-875, 2013.

[25] L. Jennings, K. L. Teo, M. Fisher, and C. J. Goh. "MISER3 Version 2, Optimal Control Software, Theory and User Manual." Perth, Western Australia: The University of Western Australia, 1997.

[26] F. Yang, K. L. Teo, R. Loxton, V. Rehbock, B. Li, C. Yu, and L. Jennings, "VISUAL MISER: An efficient user-friendly visual program for solving optimal control problems," *Journal of Industrial & Management Optimization*, vol. 12, no. 2, pp. 781-810, 2015.

[27] R. Mahony, V. Kumar, and P. Corke, "Multirotor aerial vehicles: Modeling, estimation, and control of quadrotor," *IEEE Robotics & Automation Magazine*, vol. 19, no. 3, pp. 20-32, Sept. 2012.

[28] M. Omid and M. Saleh, "Adaptive sliding mode control for finite-time stability of quad-rotor UAVs with parametric uncertainties," *ISA Transaction*, vol. 72, pp. 1-14, Jan. 2018.

This article has been accepted for publication in IEEE Transactions on Wireless Communications. This is the author's version which has not been fully edited and content may change prior to final publication. Citation information: DOI 10.1109/TWC.2021.3131384, IEEE Transactions on Wireless Communications

15

[29] A. Filippone, "Flight performance of fixed and rotary wing aircraft," *Washington, DC, USA:AIAA*, 2006.

[30] D. Shi, X. Dai, X. Zhang, and Q. Quan, "A practical performance evaluation method for electric multicopters," *IEEE/ASME Transactions on Mechatronics*, vol. 22, no. 3, pp. 1337-1348, June 2017.

[31] A. Al-Hourani, S. Kandeepan, and S. Lardner, "Optimal LAP altitude for maximum coverage," *IEEE Wireless Commun. Lett.*, vol. 3, no. 6, pp. 569–572, Dec. 2014.

[32] A. Goldsmith, "Wireless Communications." *Cambridge Univ. Press*, 2005.

[33] Q. Wu, Y. Zeng, and R. Zhang, "Joint trajectory and communication design for multi-UAV enabled wireless networks," *IEEE Transactions on Wireless Communications*, vol. 17, no. 3, pp. 2109-2121, Mar. 2018.

[34] "Data of the UAV", available online at https://flyeval.com/

[35] "Data of the brushless motor", available online at https://www.alibaba.com/product-detail/T-MOTOR-MN4006-KV380-low-noise_60818022781.html

Yong Zeng (S'12-M'14) is with the National Mobile Communications Research Laboratory, Southeast University, China, and also with the Purple Mountain Laboratories, Nanjing, China. He received the Bachelor of Engineering (First-Class Honours) and Ph.D. degrees from Nanyang Technological University, Singapore, in 2009 and 2014, respectively. From 2013 to 2018, he was a Research Fellow and Senior Research Fellow at the Department of Electrical and Computer Engineering, National University of Singapore. From 2018 to 2019, he was a Lecturer at the School of Electrical and Information Engineering, the University of Sydney, Australia.

Dr. Zeng was listed as Highly Cited Researcher by Clarivate Analytics for three consecutive years (2019-2021). He is the recipient of the Australia Research Council (ARC) Discovery Early Career Researcher Award (DECRA), 2020 IEEE Marconi Prize Paper Award in Wireless Communications, 2018 IEEE Communications Society Asia-Pacific Outstanding Young Researcher Award, 2020 & 2017 IEEE Communications Society Heinrich Hertz Prize Paper Award, and 2021 China Communications Best Paper Award. He serves as an Associated Editor for IEEE Communications Letters and IEEE Open Journal of Vehicular Technology, Leading Guest Editor for IEEE Wireless Communications on "Integrating UAVs into 5G and Beyond" and China Communications on "Network-Connected UAV Communications". He is the Symposium Chair for IEEE Globecom 2021 Track on Aerial Communications, the workshop co-chair for ICC 2018-2022 workshop on UAV communications, the tutorial speaker for Globecom 2018/2019 and ICC 2019 tutorials on UAV communications.

Bin Li (M'18-SM'18) received the Bachelor degree of automation and the Master degree of control science and engineering from Harbin Institute of Technology, China, in 2005 and 2008, respectively, and received Ph.D. degree in mathematics and statistics from Curtin University, Australia, in 2011. From 2012-2014, he was a Research Associate with the School of Electrical, Electronic and Computer Engineering, the University of Western Australia, Australia. From 2014-2017, he was a Research Fellow with the Department of Mathematics and Statistics, Curtin University, Australia. From 2017-2020, he was a Research Professor with the College of Electrical Engineering, Sichuan University, China. Currently, he is a Professor with the School of Aeronautics and Astronautics, Sichuan University, China. His research interests include model predictive control, optimal control, optimization, signal processing, and wireless communications.
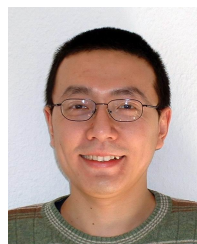
Yue Rong (S'03-M'06-SM'11) received the Ph.D. degree (summa cum laude) in electrical engineering from the Darmstadt University of Technology, Darmstadt, Germany, in 2005.

He was a Post-Doctoral Researcher with the Department of Electrical Engineering, University of California, Riverside, from February 2006 to November 2007. Since December 2007, he has been with the Department of Electrical and Computer Engineering, Curtin University, Bentley, Australia, where he is currently a Full Professor. His research interests include signal processing for communications, wireless communications, underwater acoustic communications, applications of linear algebra and optimization methods, and statistical and array signal processing. He has published over 140 journal and conference paper in these areas.

Dr. Rong was a recipient of the Best Paper Award at the 2011 International Conference on Wireless Communications and Signal Processing, the Best Paper Award at the 2010 Asia-Pacific Conference on Communications, and the Young Researcher of the Year Award of the Faculty of Science and Engineering at Curtin University in 2010. He is an Associate Editor of the IEEE Transactions on Signal Processing. He was an Editor of the IEEE Wireless Communications Letters from 2012 to 2014, a Guest Editor of the IEEE Journal on Selected Areas in Communications special issue on theories and methods for advanced wireless relays, and was a TPC Member for the IEEE ICC, WCSP, IWMC, and ChinaCom.

Qingliang Li received the Bachelor degree of science in flight vehicle control and information engineering from Sichuan University, China, in 2020. He is currently a Master student of electronic information at Sichuan University, China.

This article has been accepted for publication in IEEE Transactions on Wireless Communications. This is the author's version which has not been fully edited and content may change prior to final publication. Citation information: DOI 10.1109/TWC.2021.3131384, IEEE Transactions on Wireless Communications

16

Rui Zhang (S'00-M'07-SM'15-F'17) received the B.Eng. (first-class Hons.) and M.Eng. degrees from the National University of Singapore, Singapore, and the Ph.D. degree from the Stanford University, Stanford, CA, USA, all in electrical engineering.

From 2007 to 2010, he worked at the Institute for Infocom Research, ASTAR, Singapore. Since 2010, he has been working with the National University of Singapore, where he is now a Provost's Chair Professor in the Department of Electrical and Computer Engineering. He has published over 250 journal papers and over 190 conference papers. He has been listed as a Highly Cited Researcher by Thomson Reuters/Clarivate Analytics since 2015. His current research interests include UAV/satellite communications, wireless power transfer, reconfigurable MIMO, and optimization methods.

He was the recipient of the 6th IEEE Communications Society Asia-Pacific Region Best Young Researcher Award in 2011, the Young Researcher Award of National University of Singapore in 2015, the Wireless Communications Technical Committee Recognition Award in 2020, and the IEEE Signal Processing and Computing for Communications (SPCC) Technical Recognition Award in 2020. He received 11 IEEE Best Paper Awards, including the IEEE Marconi Prize Paper Award in Wireless Communications in 2015 and 2020, the IEEE Signal Processing Society Best Paper Award in 2016, the IEEE Communications Society Heinrich Hertz Prize Paper Award in 2017 and 2020, the IEEE Communications Society Stephen O. Rice Prize in 2021, etc. He served for over 30 international conferences as the TPC co-chair or an organizing committee member. He was an elected member of the IEEE Signal Processing Society SPCOM Technical Committee from 2012 to 2017 and SAM Technical Committee from 2013 to 2015, and served as the Vice Chair of the IEEE Communications Society Asia-Pacific Board Technical Affairs Committee from 2014 to 2015. He was a Distinguished Lecturer of IEEE Signal Processing Society and IEEE Communications Society from 2019 to 2020. He served as an Editor for the IEEE TRANSACTIONS ON WIRELESS COMMUNICATIONS from 2012 to 2016, the IEEE JOURNAL ON SELECTED AREAS IN COMMUNICATIONS: Green Communications and Networking Series from 2015 to 2016, the IEEE TRANSACTIONS ON SIGNAL PROCESSING from 2013 to 2017, and the IEEE TRANS-ACTIONS ON GREEN COMMUNICATIONS AND NETWORKING from 2016 to 2020. He is now an Editor for the IEEE TRANSACTIONS ON COMMUNICATIONS, and serves as a member of the Steering Committee of the IEEE Wireless Communications Letters. He is a Fellow of the Academy of Engineering Singapore.